Stone column settlement performance in structured anisotropic clays: the influence of creep

Cite as:

Sexton, B.G., McCabe, B.A., Karstunen, M. and Sivasithamparam, N. (2016) Stone column settlement performance in structured anisotropic clays: the influence of creep, *Journal of Rock Mechanics and Geotechnical Engineering*, Vol. 8, pp. 672-688.

[DOI: 10.1016/j.jrmge.2016.05.004]

Stone column settlement performance in structured anisotropic clays: the influence of creep

Brian G. Sexton, BE, PhD, MIEI, ***b.sexton1988@gmail.com***
PhD Student, College of Engineering and Informatics, National University of Ireland, Galway, Ireland

Bryan A. McCabe, BA, BAI, PhD, CEng, EurIng, FIEI, ***bryan.mccabe@nuigalway.ie***
Lecturer, College of Engineering and Informatics, National University of Ireland, Galway, Ireland. (Corresponding author)

Minna Karstunen, MSc, PhD, FICE, ***minna.karstunen@chalmers.se***
Professor, Chalmers University of Technology, Department of Civil and Environmental Engineering, Gothenburg, Sweden.

Nallathamby Sivasithamparam, BSc Eng, MEng, PhD, ***nallathamby.siva@ngi.no***
Project Engineer, Computational Geomechanics Division, Norwegian Geotechnical Institute, Oslo, Norway

Sponsor: Irish Research Council (IRC), EC/FP7, Swedish Transport Administration

Abstract

The recently developed elasto-viscoplastic Creep-SCLAY1S model has been used in conjunction with PLAXIS 2D to investigate the effectiveness of vibro-replacement in a creep-prone clay. The Creep-SCLAY1S model accounts for anisotropy, bonding, and destructuration, and uses the concept of a constant rate of viscoplastic multiplier to calculate creep strain rate. A comparison of settlement improvement factors with and without creep indicates that 'total' settlement improvement factors (primary plus creep) are lower than their 'primary' counterparts (primary settlement only). The lowest settlement improvement factors arise for analyses incorporating the effect of bonding and destructuration. Examination of the variations of vertical stress with time and depth has indicated that vertical stress is transferred from the soil to the column as the soil creeps. This results in additional column yielding. In addition, the radial and hoop stresses in the soil are lower for the 'creep' case. The reduced radial stresses lead to additional column bulging and hence more settlement, whereas the hoop stress reductions appear to be a secondary effect, caused by additional plastic deformation for the 'creep' case.

Keywords

Stone Columns; Creep; Anisotropy; Destructuration; Finite Element Method.

1. Introduction

Vibro-replacement has traditionally been considered to be an effective means of improving the bearing capacity and settlement characteristics of mixed fills and weak soils. Vibro-replacement solutions can be more cost-effective, quicker to implement and less CO_2-intensive than piling alternatives in certain circumstances. The technique is becoming increasingly popular for the treatment of soft fine-grained deposits; some of these soils can comprise a significant organic content, in which case creep settlements can contribute a significant proportion of the total settlement.

The settlement reduction potential of vibro stone columns is typically quantified using a settlement improvement factor (n), see Eq. 1, where $\delta_{untreated}$ and $\delta_{treated}$ are the final settlements of untreated (i.e. no columns) and treated ground respectively.

$$n = \delta_{untreated}/\delta_{treated} \quad (1)$$

The majority of analytical settlement design methods pertain to primary settlement only, e.g. Priebe (1995), Castro & Sagaseta (2009) and Pulko *et al.* (2011), and so the same n value tends to be applied to both primary and creep settlements in routine designs. In addition, the majority of n values measured in the field (McCabe *et al.* 2009) tend to be 'lumped', with no distinction between initial compression, primary consolidation settlement, and creep. The length of time required to measure 'pure' long-term creep settlements in soft low permeability soils serves as the main impediment in the latter case.

While the majority of laboratory-scale testing carried out to date has been informative (e.g. Black *et al.* 2011), it tends to be limited by scale effects and a difficulty in replicating realistic boundary conditions. Additionally, Castro *et al.* (2013) have noted that the reconstituted soils used in laboratory testing are not fully representative of natural clay behaviour, while Mesri (1973) has pointed out that the rate of creep is lower in reconstituted soils. There are also difficulties associated with extrapolating long-term performance in the field from short-term laboratory tests (Mitchell & Kelly, 2013).

Moorhead (2013) carried out a series of laboratory tests in 1D and 3D loading chambers, and is, to the authors' knowledge, the only researcher to date to investigate the creep settlement reduction potential of vibro stone columns in the laboratory. The tests were carried out on reconstituted samples of kaolin and Belfast sleech and examined stone column behaviour for both a rigid raft and an isolated loading scenario. Although the laboratory data showed a significant amount of scatter, it was tentatively concluded that columns effectively reduced primary settlement at low bearing pressures but were ineffective at high pressures, and had only a minor influence on reducing initial compression and creep settlements. The findings need to be treated with caution because the initial conditions in the untreated and treated soil beds were different in some cases.

In this paper, a series of axisymmetric analyses carried out using the PLAXIS 2D finite element (FE) program (Brinkgreve *et al.* 2011) are reported with a view to assessing the settlement reduction potential of vibro-replacement in a structured anisotropic creep-prone clay. The Bothkennar soft clay test site in Scotland, comprising an overconsolidated crust overlying two layers of lightly overconsolidated Carse clay, has been used as a representative soil profile for the numerical analyses in this paper.

In previous studies, Sexton & McCabe (2013, 2015) carried out some preliminary numerical work using a simplified single-layer version of the multi-layer Bothkennar profile to gauge the influence of creep on settlement improvement factors. Subsequently, Sexton & McCabe (2016) extended this work to a multi-layer scenario. The commercially available Soft Soil Creep (SSC) model was used to represent the host clay behaviour in these studies. The latter study in particular provided valuable insight into the likely behaviour of stone columns in creep-prone soils and formed an important frame of reference for one using a more advanced constitutive model, such as the Creep-SCLAY1S model, which is used to model the soft clay in this paper. The Creep-SCLAY1S model (Sivasithamparam *et al.* 2013, 2015) incorporates anisotropy, bonding, and destructuration, each of which can be 'switched off' individually or in various combinations by adjusting the input parameters. The model is not yet commercially available, and therefore a user-defined model implementation into the PLAXIS FE code was used. The Hardening Soil (HS) model (Schanz *et al.* 1999) is used to represent the granular column material. For the sake of simplicity, any installation effects have been ignored.

2. Modelling creep using advanced constitutive models

2.1 Model classification

Constitutive models for describing the time-dependent behaviour of soft soils can be classified as either empirical models, rheological models, or general stress-strain-time models, each of which have been reviewed in detail by Liingaard *et al.* (2004). Empirical models are generally obtained by fitting mathematical/constitutive expressions to

experimental data whereas rheological models tend to be used to gain a conceptual understanding of time effects in soil.

General stress-strain-time models are capable of describing the rate-dependent behaviour of soils under a variety of different loading conditions. These models tend to be formulated incrementally and so are suitable for implementation within the FE method. The majority of elasto-viscoplastic general stress-strain-time models are based on overstress theory (e.g. Perzyna 1963, 1966), either *'conventional overstress*' or *'extended overstress*'. '*Extended overstress models*' are preferable to '*conventional overstress models*', see Yin *et al.* (2010).

2.2 3D elasto-viscoplastic models

2.2.1 Isotropic models

The commercially available isotropic SSC model (Vermeer *et al.* 1998, Vermeer & Neher 1999) can be classified as either an '*extended overstress model*' or a '*creep model*', as defined by Yin *et al.* (2010). '*Creep models*' use the creep coefficient, C_α, or its isotropic equivalent, μ^*, as the soil viscosity input parameter. The isotropic EVP model developed by Yin *et al.* (2002) is also denoted a '*creep model*'.

2.2.2 Anisotropic models

Anisotropic elasto-viscoplastic soil models have been developed as extensions to the EVP and SSC models, e.g. the anisotropic EVP model (Zhou *et al.* 2005) and the Anisotropic Creep Model (ACM, Leoni *et al.* 2008), respectively. These '*creep models*' assume that the

viscoplastic volumetric strain rate is independent of the stress state, and consequently they predict unrealistic strain-softening behaviour for undrained triaxial tests on isotropically consolidated samples (Yin *et al.* 2010, Sivasithamparam *et al.* 2014, 2015). To overcome this deficiency, Yin *et al.* (2010) proposed a new anisotropic elasto-viscoplastic soil model in which the volumetric strain rate is dependent on the stress ratio, $\eta = q/p'$ (where p' and q denote the mean effective stresses and deviator stresses respectively).

2.2.3 Anisotropic models with bonding and destructuration

The Creep-SCLAY1S model (Sivasithamparam *et al.* 2015) is an anisotropic soil model that also takes account of bonding and destructuration. 'Destructuration' refers to the progressive breakdown/degradation of bonds during straining (Leroueil *et al.* 1979) and is accommodated using the concept of an intrinsic yield surface proposed by Gens & Nova (1993). Other models which fit in this category are the AniCreep model developed by Yin *et al.* (2011) as an extension to the model developed by Yin *et al.* (2010), the EVP-SCLAY1S model (Yin & Karstunen 2008) which is categorised as a '*conventional overstress model*', and the non-associated structured anisotropic creep (n-SAC) model, developed by Grimstad *et al.* (2010).

The key feature of the n-SAC model is that the time resistance concept is introduced on the viscoplastic multiplier rather than on the viscoplastic volumetric strain. Models which assume constant contours of volumetric creep strain (e.g. SSC or ACM) yield unrealistic creep strains for almost all stress paths (Olsson, 2013). In keeping with the n-SAC model, the Creep-SCLAY1S model also uses the concept of a constant rate of viscoplastic multiplier to calculate creep strain rate, but the commonly used semi-logarithmic creep coefficient, C_α, is

used as the viscosity input parameter, making the model attractive from a practical modelling perspective.

3. Formulation of the Creep-SCLAY1S model

The formulation of the Creep-SCLAY1S model (in triaxial stress space) is described by Sivasithamparam *et al.* (2013) and it was extended to 3D for FE analyses by Sivasithamparam *et al.* (2015). In the version used in this paper, destructuration has also been incorporated. The anisotropy and destructuration components of the model are formulated using the constitutive equations from the rate independent S-CLAY1 (Wheeler *et al.* 1997, 2003) and S-CLAY1S (Koskinen *et al.* 2002, Karstunen *et al.* 2005) models, which account for anisotropy and both anisotropy and destructuration respectively.

For the sake of simplicity, the Creep-SCLAY1S model is briefly explained here in triaxial stress space. For the extension to 3D, readers can refer to Sivasithamparam *et al*. (2015). The total strain rate ($\dot{\varepsilon}$) is composed of an elastic component ($\dot{\varepsilon}^e$) and a viscoplastic (creep) component ($\dot{\varepsilon}^c$), see Eq. 2.

$$\dot{\varepsilon} = \dot{\varepsilon}^e + \dot{\varepsilon}^c \tag{2}$$

The rotational hardening law, describing the changing inclination of the yield surface due to creep strains, takes the form shown in Eq. 3, where ω and ω_d are two additional soil constants, $d\varepsilon_v^c$ and $d\varepsilon_d^c$ are the increments of creep volumetric and deviatoric strains respectively, and $\langle\ \rangle$ denote Macaulay brackets. ω_d controls the relative effectiveness of the deviatoric and volumetric creep strains in determining the overall target value for α, while ω

controls the absolute rate at which α approaches the target value, where α is the angle of inclination of the yield surface (Figure 1).

$$d\alpha = \omega\left(\left(\frac{3\eta}{4} - \alpha\right)\left\langle d\varepsilon_v^c \right\rangle + \omega_d\left[\frac{\eta}{3} - \alpha\right]\left|d\varepsilon_d^c\right|\right) \tag{3}$$

The destructuration law describing the breakdown of bonding caused by creep strains takes the form shown in Eq. 4, where ξ and ξ_d are two additional soil constants controlling the absolute rate of destructuration and the relative effectiveness of volumetric and deviatoric creep strains respectively, in destroying the bonding.

$$d\chi = -\xi\chi\left(\left|d\varepsilon_v^c\right| + \xi_d\left|d\varepsilon_d^c\right|\right) \tag{4}$$

The initial amount of bonding (χ_0) relates the size of the natural yield surface (p'_{p0}) to the size of the intrinsic yield surface (p'_{p0i}), see Eq. 5.

$$p'_{p0} = (1 + \chi_0)\, p'_{p0i} \tag{5}$$

The yield surface ('normal consolidation surface', NCS) evolves with creep volumetric strains according to Eq. 6, with the equivalent mean stress measure (p'_{eq}, Eq. 7) defining the intersection of the current stress surface (CSS) with the p' axis (Figure 1). $M(\theta)$ is the stress ratio at critical state, which has been made a function of Lode Angle (θ) to incorporate a smooth failure surface, see Sivasithamparam *et al.* (2015), and λ^* and κ^* are the modified compression and swelling indices, and hence related to the 1D compression and swelling indices (C_c and C_s).

$$p'_p = p'_{p0} \exp\left(\frac{\varepsilon_v^c}{\lambda^* - \kappa^*}\right) \tag{6}$$

$$p'_{eq} = p' - \frac{(q - \alpha p')^2}{(M^2(\theta) - \alpha^2)p'} \tag{7}$$

In contrast to the SSC model and the ACM, which calculate the volumetric creep strain rate according to Eq. 8, the Creep-SCLAY1S model uses the rate of viscoplastic multiplier ($\dot{\Lambda}$), see Eq. 9. The additional term in Eq. 9 was added to ensure that under oedometric conditions, the resulting volumetric creep strain corresponds to Eq. 8. α_{K0nc} denotes the inclination of the yield ellipse in the normally consolidated condition and τ is a reference time, which is usually 1 day if μ^* is calculated using an incremental load oedometer test with a loading duration of 1 day.

$$\dot{\varepsilon}_v^c = \frac{\mu^*}{\tau}\left(\frac{p'_{eq}}{p'_p}\right)^{\frac{\lambda^* - \kappa^*}{\mu^*}} \tag{8}$$

$$\dot{\Lambda} = \frac{\mu^*}{\tau}\left(\frac{p'_{eq}}{p'_p}\right)^{\frac{\lambda^* - \kappa^*}{\mu^*}} \left(\frac{M^2(\theta) - \alpha^2_{K_0^{nc}}}{M^2(\theta) - \eta^2_{K_0^{nc}}}\right) \tag{9}$$

The determination of the additional model parameters required for the Creep-SCLAY1S model is straight-forward. The anisotropy parameters, α_0 (initial yield surface inclination) and ω_d can be calculated from the critical state friction angle (ϕ') and the coefficient of lateral earth pressure in the normally consolidated condition (K_0^{nc}). The value for ω should be calculated/optimised by simulating undrained triaxial extensions tests, or in their absence, simply estimated based on compressibility (Zentar *et al.* 2002).

The initial amount of bonding, χ_0, can be calculated based on the sensitivity, S_t, see Eq. 10, and the other destructuration parameters (ξ_d and ξ) can be calibrated using the optimisation procedure described in Koskinen *et al.* (2002). The intrinsic compression and creep indices, λ_i* and μ_i* (measured from oedometer tests on reconstituted samples), should be used as opposed to λ* and μ* (measured from oedometer tests on natural samples) when modelling destructuration using the FE method.

$$\chi_0 = S_t - 1 \tag{10}$$

4. Soil profile

4.1 Soil parameters

The Bothkennar soft clay test site in Scotland was purchased by the UK Science and Engineering Research Council (SERC) in 1987 as a national soft clay test bed. The silty clay at Bothkennar is highly structured with an organic content of between 3% and 5%, depending on the 'facies' type (bedded, laminated, mottled and weathered), e.g. Paul *et al.* (1992), and a bulk unit weight of γ = 16.5kN/m^3, e.g. Nash *et al.* (1992a). The multi-layer soil profile (Table 1) adopted in this study is based on the HS model soil profile used by Killeen & McCabe (2014). The authors obtained the parameters from ICE (1992) and validated their profile against a field load test on an unreinforced rigid pad footing described by Jardine *et al.* (1995). However, creep was not considered in their study and so the additional creep parameters in Table 1 were calculated based on a C_α/C_c (= μ*/λ*) ratio of 0.04, e.g. Nash *et al.* (1992b). The additional anisotropy and destructuration parameters for Bothkennar clay quoted in Table 2 have previously been calibrated by Karstunen *et al.* (2013).

The initial stress state for the FE model has been generated using a pre-overburden pressure (POP = σ'_p - σ'_0) of 15kPa for the upper layers and an overconsolidation ratio (OCR = σ'_p/σ'_0) of 1.5 for the lower Carse clay, with σ'_0 and σ'_p denoting the initial effective stresses and 1D preconsolidation stresses respectively. The *in-situ* at-rest earth-pressure coefficients (K_0) are based on a series of spade cell, self-boring pressuremeter (SBPM), and Marchetti dilatometer tests carried out by Nash *et al.* (1992a).

The slopes of the Critical State Lines in compression (M_c) and extension (M_e) have been selected based on a series of triaxial stress paths tests on reconstituted clay carried out by Allman & Atkinson (1992). M_c corresponds to a critical state friction angle of 34^o; this high friction angle is attributable to both a high organic content and an abundance of silt-sized grains. Nominal cohesion values (c' = 1kPa) have been used for numerical stability and a dilatancy angle (ψ) of 0^o was adopted as representative of a lightly overconsolidated clay. The horizontal and vertical permeabilites (k_x and k_y) were measured by Leroueil *et al.* (1992) using both *in-situ* (e.g. pushed-in-place piezometers, self-boring permeameters, BAT system) and laboratory (e.g. oedometer cells, triaxial cells, radial flow cells) methods.

The adopted soil parameters, which have been derived predominantly from the results of oedometer tests, have been validated by using the PLAXIS 'Soil Test' facility to simulate the undrained triaxial compression tests reported by Atkinson *et al.* (1992), see Sexton (2014).

4.2 Scenarios

Three separate scenarios have been considered for the Creep-SCLAY1S model analyses described in Section 6:

(i) Anisotropy and destructuration have been 'switched off' by setting the relevant parameters to zero and by setting $M_e = M_c$. For these 'isotropic' analyses, the rotational hardening law (Eq. 2) is 'switched off' and K_0 will be overpredicted, analogous to the Modified Cam Clay (MCC) model.

(ii) Anisotropy has been 'switched on' while destructuration is 'switched off'.

(iii) Both the anisotropy and bonding/destructuration parameters have been 'switched on'. The intrinsic compression and creep indices quoted in Table 1 have been used for the analyses incorporating destructuration.

ISO is used hereafter to denote the isotropic response of the Creep-SCLAY1S model with anisotropy and destructuration 'switched off', ANIS is used to denote the anisotropic response with destructuration 'switched off', and A&D denotes the response with both anisotropy and bonding/destructuration 'switched on'.

5. Modelling stone columns using the finite element method (FEM)

5.1 Previous numerical studies

The majority of numerical studies investigating stone column behaviour have used 2D analysis techniques, e.g. plane strain (Gäb *et al.* 2008) or axisymmetry (Ambily & Gandhi 2007); 3D modelling has been used by Weber *et al.* (2008), Kamrat-Pietraszewska & Karstunen (2009), and Killeen & McCabe (2014). In the majority of cases, either the Mohr Coulomb (MC) or HS models have been used to represent the behaviour of both the granular column material and the treated soil (e.g. Ellouze & Bouassida 2009, Killeen & McCabe 2014). Kamrat-Pietraszewska & Karstunen (2009) used the MCC, S-CLAY1, and S-

CLAY1S models for the soil and the HS model for the column. Kamrat-Pietraszewska (2011) and Sexton & McCabe (2013) were among the first to use a model incorporating viscous effects with an application to stone columns.

The majority of numerical studies investigating stone column behaviour have declined to use interface elements at the boundary between the granular column material and the *in situ* soil (e.g. Ambily & Gandhi 2007, Domingues *et al.* 2007a,b, Gäb *et al.* 2008), consistent with field observations that columns are tightly interlocked with the surrounding soil due to the lateral displacement caused by re-lowering the poker during column installation, e.g. McCabe *et al.* (2009). This assumption of full contact at the column-soil interface is adopted in this study.

5.2 Axisymmetric unit cell concept

The axisymmetric unit cell concept is used in this paper, representative of the behaviour of a large grid of regularly-spaced columns subjected to a uniform load, as would be used to support an embankment or a large floor slab, for example. The extent of treatment is usually measured using the area-replacement ratio, A_c/A (Eq. 11), where A_c is the cross-sectional area of a single stone column and A is the cross-sectional area of its 'unit cell'; s and D_c denote the column spacing and column diameter respectively and k is a constant depending on the column arrangement, see Figure 2. The boundary conditions applied to the unit cell are shown in Figure 3.

$$\frac{A_c}{A} = \frac{1}{k}\left(\frac{D_c}{s}\right)^2 \tag{11}$$

5.3 Stone column material parameters

The hyperbolic elasto-plastic HS model has been used to model the column material. The parameters have also been derived from Killeen & McCabe (2014), see Table 3. The model has two yield surfaces; a shear hardening yield surface to incorporate shear hardening and a cap yield surface for compression hardening. The sizes of these yield surfaces are governed by the secant (E_{50}) and oedometric (E_{oed}) moduli respectively; the unload-reload modulus, E_{ur}, is used to control the elastic unload-reload behaviour. The model accounts for the stress dependency of soil stiffness using a power law (Eq. 12), where m is the power dictating the stress dependency of soil stiffness and E_{ref} is a reference stiffness modulus corresponding to a reference pressure, p_{ref}.

$$E = E^{ref}\left(\frac{p}{p^{ref}}\right)^{m} \tag{12}$$

6. Axisymmetric 2D modelling

The impact of creep on stone column settlement performance is examined by performing two sets of analyses; one set using the standard soil properties in Table 1 and the other using very low creep coefficients ($\mu^* \lesssim 1\%$ of the standard value), in effect eliminating most of the creep effects. It is not possible to use $\mu^* = 0$ as it would result in division by zero.

These two sets of analyses (referred to subsequently as ‘creep’ and ‘no creep’) are carried out with a view to deriving settlement improvement factors (n values) for the three separate scenarios laid out in Section 4.2:

(i) The n values with and without creep for the isotropic case are denoted $n_{TOTAL(ISO)}$ and $n_{PRIMARY(ISO)}$ respectively.

(ii) The n values with and without creep for the anisotropic case are denoted $n_{TOTAL(ANIS)}$ and $n_{PRIMARY(ANIS)}$ respectively. Direct comparison with the isotropic results enables the influence of anisotropy to be established.

(iii) The n values with and without creep for the analyses incorporating anisotropy, bonding, and destructuration are denoted $n_{TOTAL(A\&D)}$ and $n_{PRIMARY(A\&D)}$ respectively. The influence of soil destructuration can then be examined.

The variations of radial, vertical, and hoop stress with time and depth corresponding to scenarios (i)-(iii) can be expounded.

The general analysis stages are as follows:

(i) Generate initial stresses using the K_0 procedure (Brinkgreve *et al.* 2011).

(ii) Install the stone columns in undrained conditions using the 'wished-in-place' technique (any changes in stresses and state parameters due to column installation are not accounted for). Any out-of-equilibrium stresses generated by the 'wished-in-place' installation are restored using a plastic nil-step.

(iii) Apply a load (p_a) of 100kPa in undrained conditions through a plate element placed over the surface of the unit cell. The plate acts as a loading platform and prevents differential settlements at the surface between the column and the soil.

(iv) Allow a consolidation phase; settlements effectively cease after full pore pressure dissipation for the 'no creep' case.

7. Computational Results and Discussion

7.1 Time-settlement behaviour

Settlement versus time plots in logarithmic scale for the untreated 'creep' and 'no creep' cases for the three different scenarios are presented in Figure 4. The time-settlement behaviour for the isotropic and anisotropic cases is almost identical. This will be the case for 1D loading if the anisotropy parameters are derived based on the K_0 state. The EOP consolidation times for the 'no creep' and 'creep' cases are approximately 15,000 days (~40 years) and 40,000 days (~100 years) respectively. The EOP consolidation times are shorter and settlements are lower for the case with bonding and destructuration (since $\lambda_i^* << \lambda^*$ and $\mu_i^* << \mu^*$).

The time-settlement behaviour for the treated case (at different reciprocal area-replacement ratios, A/A_c) is compared to that of the untreated case in Figures 5a and 5b for the 'no creep' and 'creep' cases respectively; these plots pertain to the isotropic case. It is evident that the granular columns significantly accelerate the consolidation process; the consolidation time reduces with increasing stone replacement. The findings are consistent with those reported by Kok Shien (2013), who also modelled stone columns using the axisymmetric unit cell concept, albeit using a different soil model and soil profile. Settlement-log time plots for the 'anisotropy' and 'anisotropy and destructuration' cases are not presented here because the patterns are relatively consistent with the isotropic case; settlement differences will be reflected in the relevant *n* values.

7.2 Evolution of settlement improvement factor with time

The evolution of n with time for the 'creep' and 'no creep' cases is plotted in Figure 6 for the different scenarios; $A/A_c = 6$ is chosen for illustrative purposes. In all cases, the predicted n values are less than unity initially because the settlement of treated ground occurs more rapidly than that of untreated ground; however, these n values are of no practical significance. Regardless of the scenario, the 'steady-state' n_{TOTAL} values after EOP are less than the corresponding $n_{PRIMARY}$ values; this holds at all values of A/A_c and is consistent with the findings of Sexton & McCabe (2013, 2015, 2016): when creep is present, n values are lower than would be obtained had primary consolidation been considered alone.

7.3 Comparison of settlement improvement factors

The $n_{PRIMARY}$ and n_{TOTAL} values (after EOP) for the different scenarios are presented in Figures 7a and 7b, respectively. At all values of A/A_c, the highest n values arise for the isotropic case and the lowest for the analyses incorporating bonding and destructuration. For the isotropic analyses, K_0 is overpredicted (see Section 4.2), resulting in larger horizontal soil stresses which provide more resistance against column bulging. This results in lower settlements for the treated case, and since the settlements of untreated soil for the isotropic and anisotropic cases are similar, $n_{PRIMARY(ISO)} > n_{PRIMARY(ANIS)}$.

For the analyses incorporating bonding and destructuration ($\lambda_i^* << \lambda^*$ and $\mu_i^* << \mu^*$), the ratio of column stiffness to soil stiffness is lower and slightly lower n values would be expected. However, the n values in Figures 7a and 7b are still much lower than would be expected because n is not very sensitive to soil stiffness (and hence the ratio of column

stiffness to soil stiffness) above a threshold value, e.g. Kirsch (2004). The lower *n* values can be explained as follows:

(i) Increased settlement leads to a reduction to the bonding parameter, χ.

(ii) Creep (i.e. more settlement) leads to additional bond degradation (for both the untreated and treated cases), and hence a larger reduction to χ.

(iii) For the 'no creep' case, columns reduce settlement to a larger extent than they do for the 'creep' case (and hence they curtail the amount by which χ is reduced).

The extent to which destructuration should be accounted for in design will depend on the initial amount of bonding, χ_0, which is dictated by the soil sensitivity, S_t (see Eq. 9).

Analytical predictions obtained using Priebe (1995), Castro & Sagaseta (2009), and Pulko *et al.* (2011) are superimposed with the $n_{PRIMARY}$ values in Figure 7a for comparison. The *n* values predicted by Castro & Sagaseta (2009) and Pulko *et al.* (2011) fall between the $n_{PRIMARY(ISO)}$ and $n_{PRIMARY(ANIS)}$ for $4 < A/A_c < 15$.

'Creep' settlement improvement factors for the different scenarios are compared in Figure 7c. These 'creep' settlement improvement factors have been derived based on the slopes of the settlement-log(time) plots after EOP: $n_{CREEP} = \mu^*_{untreated}/\mu^*_{treated}$, where $\mu^*_{untreated}$ and $\mu^*_{treated}$ denote the slopes of the untreated and treated settlement-log(time) plots respectively. For each scenario considered, these n_{CREEP} values are lower than the corresponding $n_{PRIMARY}$ values. However, given the n_{CREEP} values are greater than 1.0, the columns have a positive impact on reducing long-term creep settlements. The n_{TOTAL} values in Figure 7b are effectively a weighted average of the $n_{PRIMARY}$ and n_{CREEP} values, dependent on the relative

percentages of primary/creep settlement. In general, larger differences between $n_{PRIMARY}$ and n_{TOTAL} would be observed in situations where $n_{PRIMARY}$ is larger to begin with. This occurs because the $n_{PRIMARY}$ values are much greater than the n_{CREEP} values and so a larger effect would be seen in the weighted average.

The relative differences between the n_{TOTAL} and $n_{PRIMARY}$ values for each scenario are investigated in Figure 8 by plotting (n_{TOTAL} - 1) against ($n_{PRIMARY}$ - 1) at different values of A/A_c; for an untreated soil, both n_{TOTAL} and $n_{PRIMARY}$ will be equal to 1. Each datapoint in Figure 8 corresponds to a $n_{PRIMARY}$ value and a n_{TOTAL} value at a single value of A/A_c. Best-fit lines have been added to each figure, along with their corresponding coefficients of determination (R^2). The relationship takes the form shown in Eq. 13, where β is the slope of the line. For the isotropic and anisotropic cases, the β values are almost identical, suggesting that the relative values of n_{TOTAL} and $n_{PRIMARY}$ are rather independent of anisotropy. For the case incorporating anisotropy and bonding/destructuration, the value of β is higher because (i) the $n_{PRIMARY(A\&D)}$ values are lower to begin with and (ii) $\mu_i^* << \mu^*$ so the weighted effect of creep is less visible.

$$(n_{TOTAL} - 1) = \beta . (n_{PRIMARY} - 1) \tag{13}$$

7.4 Variations of vertical, radial, and hoop stress with time

For the 'no creep' case, the stresses on the soil and column are constant after EOP. For the 'creep' case, vertical stress is transferred from the soil to the column as the soil creeps. This is illustrated in Figure 9 by plotting the variations of vertical stress (σ'_{yy}) with time for A/A_c = 3 (for the isotropic case) at points C and S (mid-depth of the lower Carse clay layer) in Figure

3. The spacing represented by A/A_c = 3 has been selected for presentation purposes because the stress transfer is most pronounced at close spacings, although the same trend holds for the range 3 < A/A_c < 15 considered. The additional stress transferred to the already yielded column results in additional yielding, and hence lower *n* values for the 'creep' case.

The corresponding variations of radial (σ'_{xx}) and hoop (σ'_{zz}) stress in the soil with time are plotted in Figures 10a and 10b respectively. For the 'no creep' case, both σ'_{xx} and σ'_{zz} are constant after EOP. For the 'creep' case, these stresses continue to reduce after EOP, with σ'_{zz} reducing to a greater extent than σ'_{xx}. The reduction in σ'_{xx} means that the lateral support imparted onto the column by the soil diminishes due to creep. This leads to additional column bulging, more settlement, and ultimately, a lower load-carrying capacity. The σ'_{xx} and σ'_{zz} reductions will be discussed in more detail in Sections 7.5.2 and 7.5.3.

7.5 Profiles of stress and strain with depth

In this section, distributions of stress and strain with depth in the soil for A/A_c = 3 (with and without creep) are compared after 100 years (after EOP for the untreated case) to highlight the effect of the different features (e.g. anisotropy, bonding and destructuration). The stress and strain profiles have been obtained at the same radius from the column centre as a vertical plane through point S in Figure 3.

7.5.1 Vertical stress profiles

The vertical stress profiles in the soil for A/A_c = 3 are plotted in Figure 11 for the different scenarios without and with creep respectively. The stress profiles for the untreated case are

also included on the figure to provide a frame of reference for comparison between the 'creep' and 'no creep' cases. The Updated Mesh option (e.g. McMeeking & Rice 1975) has been used for these analyses and so the final ground surface will be 'lower' when there is more settlement, e.g. for the analyses incorporating creep.

For each scenario, the columns reduce the vertical stress carried by the soil over the full column length in comparison with the untreated case. For the 'creep' case (Figure 11b), the stress reductions are larger and increase with depth. These are illustrated using arrows and markers for visual purposes. The surplus stress unloaded from the soil is transferred to the column, as discussed in Section 7.4. The stress transfer (i.e. the stress reduction in the soil) is smallest for the analyses incorporating destructuration (Figure 11b) because of the lower creep coefficient (i.e. $\mu_i^* << \mu^*$).

7.5.2 Radial stress profiles

The corresponding radial stress profiles in the soil for A/A_c = 3 are presented in Figure 12; reference lines (with no physical significance) have been included on this figure for ease of comparison between the 'creep' and 'no creep' cases. The stress profiles for the untreated case have not been included on these figures for the sake of clarity; the radial stresses in the soil for the untreated case are almost equivalent to those in the soil for the 'no creep' case, see Figure 12a, apart from the isotropic case, for which the untreated radial stresses are overpredicted. For the 'creep' case (Figure 12b), the radial stresses in the soil are lower than for the 'no creep' case (Figure 12a).

The magnitudes of the radial stress reductions are relatively consistent for the three scenarios considered, although there are significant stress oscillations for the 'creep' case. These oscillations are caused by shear-plane formation in the column (due to additional yielding, e.g. Figure 13, illustrated for the isotropic case) and extend much deeper for the anisotropic case than for the isotropic case. For the isotropic case, the horizontal stresses in the soil are overpredicted and so additional resistance is provided against lateral column bulging; this inhibits the formation of shear-planes in the column. The magnitudes of the shear-planes are similar for the 'anisotropy and destructuration' case, despite the lower creep coefficient ($\mu_i^* << \mu^*$); for this scenario, columns do not have the same beneficial effect on χ, as discussed in Section 7.3.

The shear-plane formations can also be identified by examining profiles of radial strain (ε_{xx}) in the soil with depth (Figure 14). For the 'creep' case, there is a sharp decrease of radial strain at the base of the unit cell (Figure 14b); this explains the 'jump' in the radial stress profile at the base in Figure 12b. Additional analysis have shown that these 'jumps' also occur at the base of floating columns; floating columns punch into the underlying soil and so there is also a sudden lateral/radial strain reduction. This is illustrated in Figure 15 for the isotropic case.

7.5.3 Hoop stress profiles

The corresponding distributions of hoop stress in the soil with depth for A/A_c = 3 are presented in Figure 16. The plots are presented in a similar format to those for radial stress. The hoop stresses are equal to the radial stresses for the untreated case. The following points are relevant:

- The hoop stresses in the soil are lower than the radial stresses (comparing Figure 16 with Figure 12) and hence lower than the corresponding hoop stresses in the soil for the untreated case.
- The hoop stress reductions for the 'no creep' case are more prominent in regions where the strains are largest, e.g. at the depth of maximum column bulging (which can be approximated from Figures 13 and 14 as being between 3m and 4m below ground level). The hoop stress reductions are caused by plastic deformation which leads to the dissipation of energy; there is more plastic deformation at the bulging depth than at the base.
- The hoop stress reductions are larger for the 'creep' case (Figure 16b) because there is more plastic deformation throughout the full depth of the profile. A larger hoop stress reduction occurs for the anisotropic case than for the isotropic case (additional plastic deformation and shear plane formation leads to a larger hoop stress reduction, e.g. Figure 14b). The hoop stress profile for the analyses incorporating anisotropy and bonding/destructuration is approximately parallel to that for the anisotropic case, although the hoop stress reduction is lower (less plastic deformation because $\mu_i^* << \mu^*$, e.g. Figure 14b).

8. Conclusions and recommendations for future research

A series of axisymmetric analyses have been carried out in conjunction with the elasto-viscoplastic Creep-SCLAY1S model to assess the effectiveness of stone columns in soft creep-prone soils. The columns were wished-in-place and hence installation effects have not been accounted for. Three different scenarios have been considered; (i) isotropy, (ii)

anisotropy, and (iii) anisotropy and bonding/destructuration. The main findings are as follows:

- For all three scenarios, incorporating creep leads to lower 'total' settlement improvement factors than would be obtained had primary consolidation been considered alone, i.e. 'primary' settlement improvement factors. The 'total' settlement improvement factors are effectively a weighted average of 'primary' and 'creep' settlement improvement factors; the latter are much lower than the former but are, nevertheless, greater than unity. If creep constitutes a significant proportion of total settlement, lower settlement improvement factors for creep settlements should be used in design.
- The ratios of 'total' to 'primary' settlement improvement factors are almost identical for the 'isotropic' and 'anisotropic' cases, suggesting the effectiveness of stone columns at arresting creep settlements is independent of anisotropy. A smaller ratio is observed for the case incorporating 'anisotropy and bonding/destructuration' because (i) the 'primary' settlement improvement factors for this scenario are lower to begin with and (ii) the 'intrinsic' creep index is less than the creep index for natural clay ($\mu_i^* << \mu^*$) so the effect of creep on the weighted average is less visible.
- For the 'creep' case, vertical stress is transferred from the 'creeping' soil to the granular column. The additional vertical stress transferred to the already yielded column causes additional yielding and explains why 'total' settlement improvement factors are lower than their 'primary' counterparts.
- The actual n values (both 'primary' and 'total') are lower for the analyses incorporating bonding and destructuration. The extent to which destructuration should be accounted for in design will depend on the initial sensitivity of the clay; in highly sensitive clays, destructuration will be a greater consideration.

- In addition to the vertical stress transfer process, the radial and hoop stresses in the soil also reduce for the ‘creep’ case. The radial stress reduction results in additional column bulging and a lower load-carrying capacity. The hoop stress reduction is more of a secondary effect, caused by additional plastic deformation (and hence energy dissipation) for the ‘creep’ case.
- The simulations ignored any installation effects, which inevitably are significant (e.g. Castro & Karstunen 2010, Castro *et al.* 2014). Hence for future work, it is recommended to complement the present study with analyses that account for installation effects for a more complete understanding of how the stone columns behave in soft sensitive creep-prone soils.

Acknowledgements

The authors would like to acknowledge the funding provided by the Irish Research Council (IRC) for the research into stone column behaviour in creep-prone soils. The development of the soil model used herein was carried out as part of CREEP (Creep of Geomaterials, PIAP-GA-2011-286397) project supported by the European Community through the programme Marie Curie Industry-Academia Partnerships and Pathways (IAPP) under the 7th Framework Programme. The support from the BIG (Better Interaction in Geotechnics) project from the Swedish Transport Administration is also gratefully acknowledged.

Notation

The following symbols are used in this paper:

A = Cross-sectional area of soil unit treated with granular material

A_c = Cross-sectional area of granular column

A_c/A = Area-replacement ratio

C_s = Swelling Index

C_c = Compression Index

C_α = Coefficient of Secondary Compression / Creep Coefficient

c' = Effective Cohesion

D_c = Column Diameter

E_{50} = Secant/Triaxial Modulus

E_{oed} = Oedometric Modulus

E_{ur} = Unload-reload Modulus

e_0 = Initial void ratio

K_0 = Coefficient of lateral earth pressure at rest

K_0^{nc} = Coefficient of lateral earth pressure in the normally consolidated condition

k = Constant dependent on column arrangement (square, triangular, or hexagonal)

k, k_x, k_y = Permeability, horizontal permeability, vertical permeability

M, M_c, M = Slope of CSL, Slope of CSL in Compression, Slope of CSL in Extension

$M(\theta)$ = Stress ratio at critical state

m = Power dictating the stress dependency of soil stiffness (HS model)

n = Settlement improvement factor, $n = \delta_{untreated}/\delta_{treated}$

n_{TOTAL} = 'Total' settlement improvement factor (i.e. primary + creep)

n_{CREEP} = ‘Creep’ settlement improvement factor

$n_{PRIMARY}$ = ‘Primary’ settlement improvement factor

n_2 = Priebe’s 1995 settlement improvement factor

p, p' = Mean principal total stress, mean principal effective stress

p_a = Applied load / load level

p_p = Preconsolidation stress / pressure (3D)

p^{ref} = Reference pressure

q = Deviatoric stress

R_c = Column Radius

S_t = Sensitivity

s = Column Spacing

α_0, α = Initial yield surface inclination, yield surface inclination

γ = Bulk unit weight

δ = Settlement

ε_{xx} = Radial strain

θ = Lode Angle

κ, κ^* = Swelling Indices

λ, λ^* = Compression Indices

λ_i, λ_i^* = Intrinsic Compression Indices

μ, μ^* = Creep Coefficients/Indices

ν = Poisson’s ratio

ξ = Rate of destructuration

ξ_d = Effectiveness of shear and volumetric strains in destroying the bonding

σ'_0 = Initial effective stress / pressure (1D)

σ'_p = Preconsolidation stress / pressure (1D)

σ'_{xx}, σ'_{yy}, σ'_{zz} = Effective radial, vertical (axial), and hoop (tangential) stresses

ϕ' = Friction Angle

ω = Rate of yield surface rotation

ω_d = Effectiveness of shear and volumetric strains in rotating the yield surface

χ_0 = Initial amount of bonding

ψ = Dilatancy Angle

$\dot{\Lambda}$ = Rate of viscoplastic multiplier

References

- Allman, M. A. & Atkinson, J. H. (1992). "Mechanical properties of reconstituted Bothkennar soil." *Géotechnique*, **42**(2), 289-301.
- Ambily, A. P. & Gandhi, S. R. (2007). "Behavior of Stone Columns Based on Experimental and FEM Analysis." *J. Geotech. Geoenviron. Eng.*, **133**(4), 405-415.
- Atkinson, J. H., Allman, M. A. & Boese, R. J. (1992). "Influence of laboratory sample preparation procedures on the strength and stiffness of intact Bothkennar soil recovered using the Laval sampler." *Géotechnique*, **42**(2), 349-354.
- Black, J. A., Sivakumar, V. & Bell, A. (2011). "The settlement performance of stone column foundations." *Géotechnique*, **61**(11), 909-922.
- Brinkgreve, R. B. J., Swolfs, W. M. & Engin, E. (2011). *"PLAXIS 2D 2010."* PLAXIS B.V.
- Castro, J. & Sagaseta, C. (2009). "Consolidation around stone columns. Influence of column deformation." *Int. J. Num. Anal. Methods in Geomech.*, **33**(7), 851-877.
- Castro, J. & Karstunen, M. (2010). "Numerical simulations of stone column installation." *Canadian Geotechnical J.*, **47**(10), 1127-1138.

- Castro, J., Karstunen, M., Sivasithamparam, N. & Sagaseta, C. (2013). "Numerical analyses of stone column installation in Bothkennar clay." *Proc., Int. Conf. on Installation Effects in Geotechnical Engineering (ICIEGE)*, Rotterdam, The Netherlands, 212-218.
- Castro, J., Karstunen, M. & Sivasithamparam, N. (2014). "Influence of stone column installation on settlement reduction." *Computers and Geotechnics*, **59**, 87-97.
- Domingues, T. S., Borges, J. L. & Cardoso, A. S. (2007a). "Stone columns in embankments on soft soils. Analysis of the effects of the gravel deformability." *Proceedings of the 14th European Conference on Soil Mechanics and Geotechnical Engineering*, Madrid, Spain, 1445-1450.
- Domingues, T. S., Borges, J. L. & Cardoso, A. S. (2007b). "Parametric study of stone columns in embankments on soft soils by finite element method." *Proceedings of the 5th International Workshop on Applications of Computational Mechanics in Geotechnical Engineering*, Guimaraes, Portugal, 281-291.
- Ellouze, S. & Bouassida, M. (2009). "Prediction of the settlement of reinforced soft clay by a group of stone columns." *Proc., 2nd Int. Conf. on New Developments in Soil Mechanics and Geotechnical Engineering*, Nicosia, North Cyprus, 182-187.
- Gäb, M., Schweiger, H. F., Kamrat-Pietraszewska, D. & Karstunen, M. (2008). "Numerical analysis of a floating stone column foundation using different constitutive models." *Proc., 2nd Int. Workshop on the Geotechnics of Soft Soils - Focus on Ground Improvement*, Glasgow, 137-142.
- Grimstad, G., Degago, S. A., Nordal, S. & Karstunen, M. 2010. "Modeling creep and rate effects in structured anisotropic soft clays." *Acta Geotechnica*, **5**(1), 69-81.
- Institution of Civil Engineers. (1992). "Bothkennar soft clay test site: characterization and lessons learned." *Géotechnique*, **42**(2), 161-378.

- Janbu, N. (1969). ″The resistance concept applied to deformations of soils.″ *Proc., 7th Int. Conf. on Soil Mechanics and Foundation Engineering (ICSMFE)*, **1**, Mexico City, Mexico, 191-196.
- Jardine, R. J., Lehane, B. M., Smith, P. R. & Gildea, P. A. (1995). ″Vertical loading experiments on rigid pad foundations at Bothkennar.″ *Géotechnique*, **45**(4), 573-597.
- Kamrat-Pietraszewska, D. & Karstunen, M. (2009). ″The behaviour of stone column supported embankment constructed on soft soil.″ *Computational Geomechanics, COMGEO I - Proc., 1st Int. Symp. on Computational Geomechanics*, Juan-les-Pins, 829-841.
- Kamrat-Pietraszewska, D. (2011). *″Numerical modelling of soft soils improved with stone columns.″* PhD thesis, University of Strathclyde.
- Karstunen, M., Krenn, H., Wheeler, S. J., Koskinen, M. & Zenter, R. (2005). ″Effect of Anisotropy and Destructuration on the Behavior of Murro Test Embankment.″ *Int. J. Geomech.*, **5**(2), 87-97.
- Karstunen, M., Sivasithamparam, N., Brinkgreve, R. B. J. & Bonnier, P. G. (2013). ″Modelling rate-dependent behaviour of structured clays.″ *Proc., Int. Conf. on Installation Effects in Geotechnical Engineering (ICIEGE)*, Rotterdam, The Netherlands, 43-50.
- Killeen, M. M. & McCabe, B. A. (2014). ″Settlement performance of pad footings on soft clay supported by stone columns: A numerical study.″ *Soils and Foundations*, **54**(4), 760-776.
- Kok Shien, N. G. (2013). *″Numerical Study of Floating Stone Columns.″* PhD Thesis, National University of Singapore.

- Koskinen, M., Karstunen, M. & J., W. S. (2002). "Modelling destructuration and anisotropy of a natural soft clay." *Proc., 5th European Conf. on Numerical Methods in Geotechnical Engineering (NUMGE 2002),* Paris, 11-20.
- Landva, A. (1964). "Equipment for cutting and mounting undisturbed specimens of clay in testing devices." *Publication 56*, 1-5, Norwegian Geotechnical Institute.
- Leoni, M., Karstunen, M. & Vermeer, P. A. 2008. "Anisotropic creep model for soft soils." *Géotechnique*, **58**(3), 215-226.
- Leroueil, S., Tavenas, F., Brucy, F., La Rochelle, P. & Roy, M. (1979). "Behaviour of destructured natural clays." *J. of Geotechnical Engineering*, **105**(6), 759-778.
- Leroueil, S., Lerat, P., Hight, D. W. & Powell, J. J. M. (1992). "Hydraulic conductivity of a recent estuarine silty clay at Bothkennar." *Géotechnique*, **42**(2), 275-288.
- Liingaard, M., Augustesen, A. & Lade, P. V. (2004). "Characterization of Models for Time-Dependent Behavior of Soils." *Int. J. Geomech.*, **4**(3), 157-177.
- McCabe, B. A., Nimmons, G. J. & Egan, D. (2009). "A review of field performance of stone columns in soft soils." *Proc., ICE - Geotechnical Engineering*, **162**(6), 323-334.
- McMeeking, R. M. & Rice, J. R. (1975). "Finite-element formulations for problems of large elastic-plastic deformation." *Int. J. of Solids and Structures*, **11**(5), 601-616.
- Mesri, G. (1973). "Coefficient of Secondary Compression." *J. of the Soil Mechanics and Foundations Division*, **99**(1), 123-137.
- Mitchell, J. K. & Kelly, R. 2013. "Addressing some current challenges in ground improvement." *Proc., ICE - Ground Improvement*, **166**(3), 127-137.
- Moorhead, M. C. (2013). *"Effectiveness of Granular Columns for Containing Settlement of Foundations Supported on Soft Clay."* PhD Thesis, The Queen's University, Belfast.
- Nash, D. F. T., Powell, J. J. M. & Lloyd, I. M. (1992a). "Initial investigations of the soft clay test site at Bothkennar." *Géotechnique*, **42**(2), 163-181.

- Nash, D. F. T., Sills, G. C. & Davison, L. R. (1992b). ″One-dimensional consolidation testing of soft clay from Bothkennar.″ *Géotechnique*, **42**(2),241-256.
- Olsson, M. (2013). *″On Rate-Dependency of Gothenburg Clay.″* PhD Thesis, Chalmers University of Technology, Gothenburg, Sweden.
- Paul, M. A., Peacock, J. D. & Wood, B. F. (1992). ″Engineering geology of the Carse clay at the National Soft Clay Research Site, Bothkennar.″ *Géotechnique*, **42**(2), 183-198.
- Perzyna, P. (1963). ″The constitutive equations for work-hardening and rate sensitive plastic materials.″ *Proc., Vibration Problems Warsaw,* **4**, 281-290.
- Perzyna, P. (1966). ″Fundamental problems in viscoplasticity.″ *Advances in Applied Mechanics,* **9**(2), 244−377.
- Priebe, H. J. (1995). ″The design of vibro replacement.″ *Ground Engineering*, 28(10), 31-37.
- Pulko, B., Majes, B. & Logar, J. (2011). ″Geosynthetic-encased stone columns: Analytical calculation model.″ *Geotextiles and Geomembranes*, **29**(1), 29-39.
- Schanz, T., Vermeer, P. A. & Bonnier, P. G. (1999). ″The hardening soil model: Formulation and verification.″ *Beyond 2000 in Computational Geotechnics. Ten Years of PLAXIS Int.*, Amsterdam, 281-290.
- Sexton, B. G. & McCabe, B. A. (2013). ″Numerical modelling of the improvements to primary and creep settlements offered by granular columns.″ *Acta Geotechnica*, **8**(4), 447-464.
- Sexton, B.G. (2014). *″The influence of creep on the settlement of foundations supported by stone columns.″* PhD Thesis, National University of Ireland, Galway.
- Sexton, B. G. & McCabe, B. A. (2015). ″Modeling stone column installation in an elasto-viscoplastic soil.″ *Int. J. of Geotechnical Engineering*, **9**(5), 500-512.

- Sexton, B. G. & McCabe, B. A. (2016). "Stone column effectiveness in soils with creep: a numerical study." *Geomechanics and Geoengineering*, 10.1080/17486025.2016.1151556.
- Sivasithamparam, N., Karstunen, M., Brinkgreve, R. B. J. & Bonnier, P. G. (2013). *"*Comparison of two anisotropic models at element level*." Proc., Int. Conf. on Installation Effects in Geotechnical Engineering (ICIEGE), R*otterdam, The Netherlands, 72-78.
- Sivasithamparam, N., Karstunen, M. & Bonnier, P. (2015). *"*Modelling creep behaviour of anisotropic soft soils*." Computers and Geotechnics*, **69**, 46-57.
- Vermeer, P. A., Stolle, D. F. E. & Bonnier, P. G. (1998). *"*From the classical theory of secondary compression to modern creep analysis*." Proc., 9th Int. Conf. on Computer Methods and Advances in Geomechanics*, **4**, Wuhan, China, 2469-2478.
- Vermeer, P. A. & Neher, H. P. (1999). *"*A soft soil model that accounts for creep*." Beyond 2000 in Computational Geotechnics. Ten Years of PLAXIS Int.,* Amsterdam, 249-261.
- Weber, T. M., Springman, S. M., Gäb, M., Racansky, V. & Schweiger, H. F. (2008). *"*Numerical modelling of stone columns in soft clay under an embankment*." Proc., 2nd Int. Workshop on the Geotechnics of Soft Soils - Focus on Ground Improvement*, Glasgow, 305-311.
- Wheeler, S. J. (1997). *"*A rotational hardening elasto-plastic model for clays*." Proc., 14th Int. Conf. on Soil Mechanics and Foundation Engineering*, **1**, Hamburg, 431-434.
- Wheeler, S. J., Näätänen, A., Karstunen, M. & Lojander, M. (2003). *"*An anisotropic elastoplastic model for soft clays*." Canadian Geotechnical J.*, **40**(2), 403-418.
- Yin, J. H., Zhu, J. G. & Graham, J. (2002). *"*A new elastic viscoplastic model for time-dependent behaviour of normally and overconsolidated clays: theory and verification*." Canadian Geotechnical J.*, **39**(1), 157-173.

- Yin, Z. Y. & Karstunen, M. (2008). "Influence of Anisotropy, Destructuration and Viscosity on the Behavior of an Embankment on Soft Clay." *Proc., 12th Int. Conf. of the International Association for Computer Methods and Advances in Geomechanics (IACMAG)*, Goa, India, 4728-4735.
- Yin, Z. Y., Chang, C. S., Karstunen, M. & Hicher, P. Y. 2010. "An anisotropic elastic-viscoplastic model for soft clays." *Int. J. of Solids and Structures*, **47**(5), 665-677.
- Yin, Z. Y., Karstunen, M., Chang, C. S., Koskinen, M. & Lojander, M. (2011). "Modeling Time-dependent Behavior of Soft Sensitive Clay." *J. Geotech. Geoenviron. Eng.*, **137**(11), 1103-1113.
- Zhou, C., Yin, J. H., Zhu, J. G. & Cheng, C. M. (2005). "Elastic Anisotropic Viscoplastic Modeling of the Strain-Rate-Dependent Stress-Strain Behavior of K_0-Consolidated Natural Marine Clays in Triaxial Shear Tests." *Int. J. Geomech.*, **5**, 3, 218-232.
- Zentar, R., Karstunen, M., Wiltafafsky, C., Schweiger, H.F. & Koskinen, M. (2002). "Comparison of two approaches for modelling anisotropy of soft clays." *Proc., 8th Int. Symposium of Numerical Models in Geomechanics (NUMOG VIII)*, Rome, 115-121.

Table 1. Bothkennar material parameters

	Crust	Upper Carse Clay	Lower Carse Clay
Depth (m)	0.0 - 1.5	1.5 - 2.5	2.5 - 14.5
γ (kN/m^3)	18.0	16.5	16.5
OCR	-	-	1.5
POP	15.0	15.0	-
K_0	1.5	1.0	0.75
Initial void ratio, e_0	1.0	1.2	2.0
λ^*	0.015	0.049	0.162
λ_i^*	0.006	0.018	0.060
κ^*	0.002	0.006	0.023
μ^*	0.0006	0.0020	0.0065
μ_i^*	0.0002	0.0007	0.0024
c' (kPa)	3.0	1.0	1.0
ψ (^{o})	0	0	0
Poisson's Ratio, v	0.2	0.2	0.2
k_x (m/day)	1 x 10^{-4}	1 x 10^{-4}	1 x 10^{-4}
k_y (m/day)	6.9 x 10^{-5}	6.9 x 10^{-5}	6.9 x 10^{-5}

Table 2. Additional material parameters

M_c	M_e	α_0	ω_d	ω	χ_0	ξ_d	ξ
1.375	-1.00	0.5267	0.9281	50	8	0.2	9

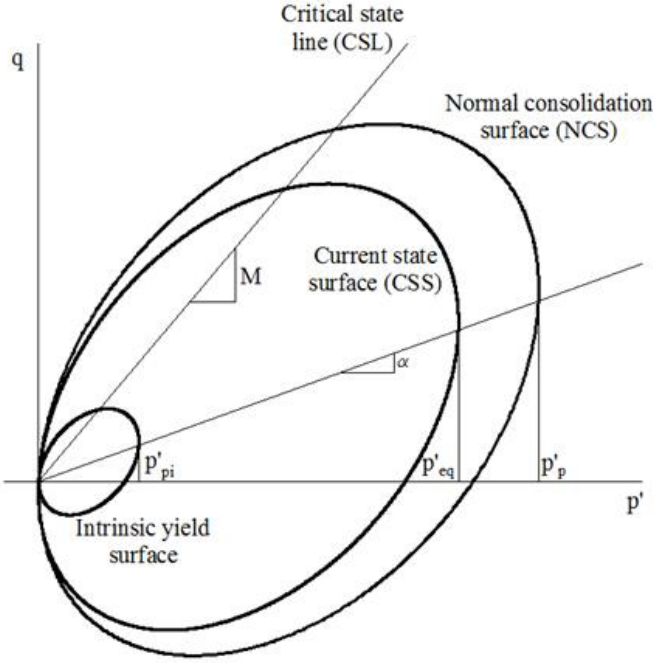

Fig. 1. Yield surfaces of the Creep-SCLAY1S model in triaxial stress space

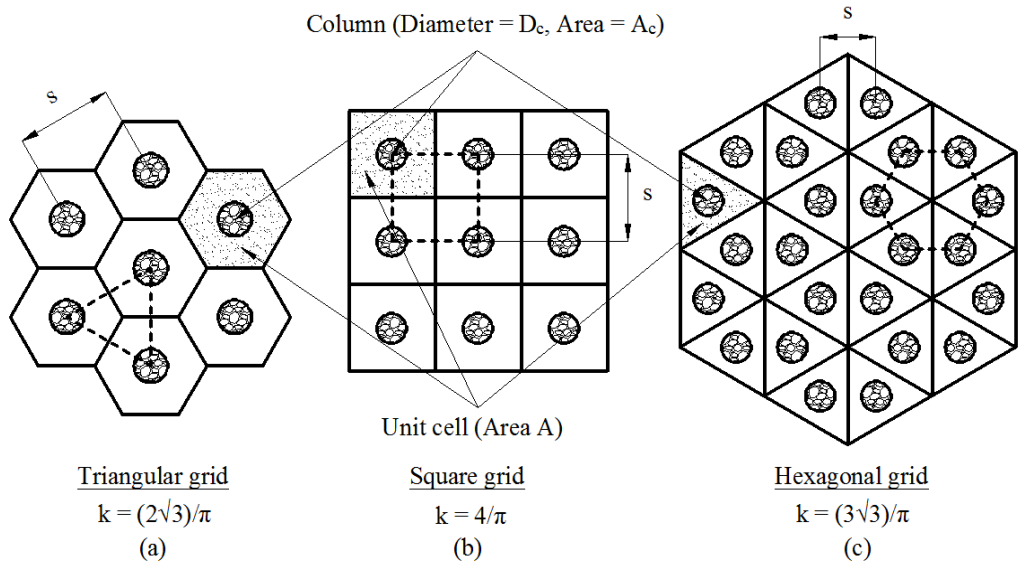

Fig. 2. Typical column grids encountered in practice; (a) triangular (b) square (c) hexagonal

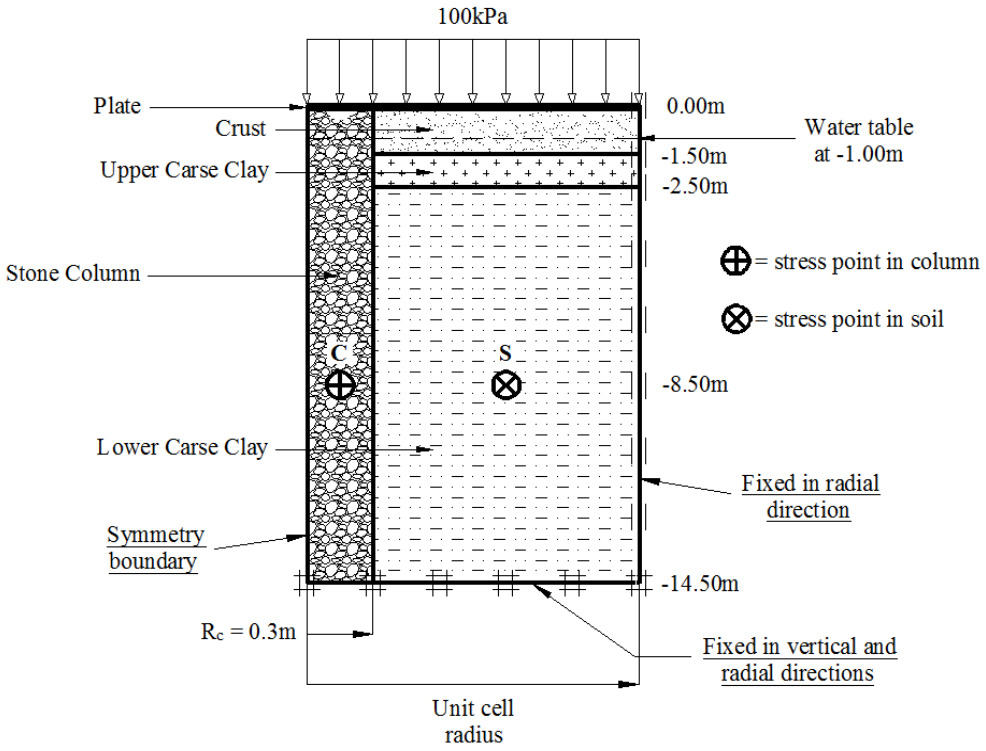

Fig. 3. Bothkennar Soil Profile (not to scale)

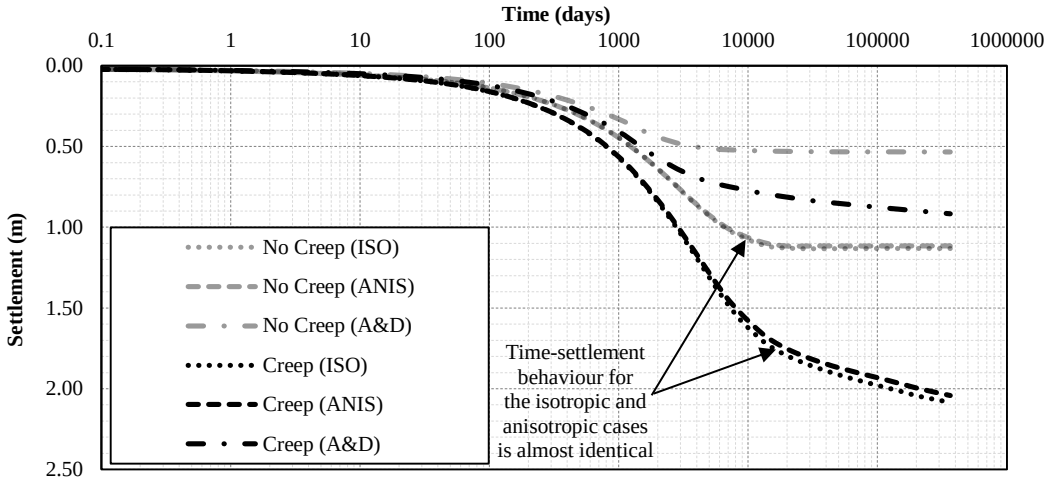

Fig. 4. Settlement vs. log(time) plots for untreated soil

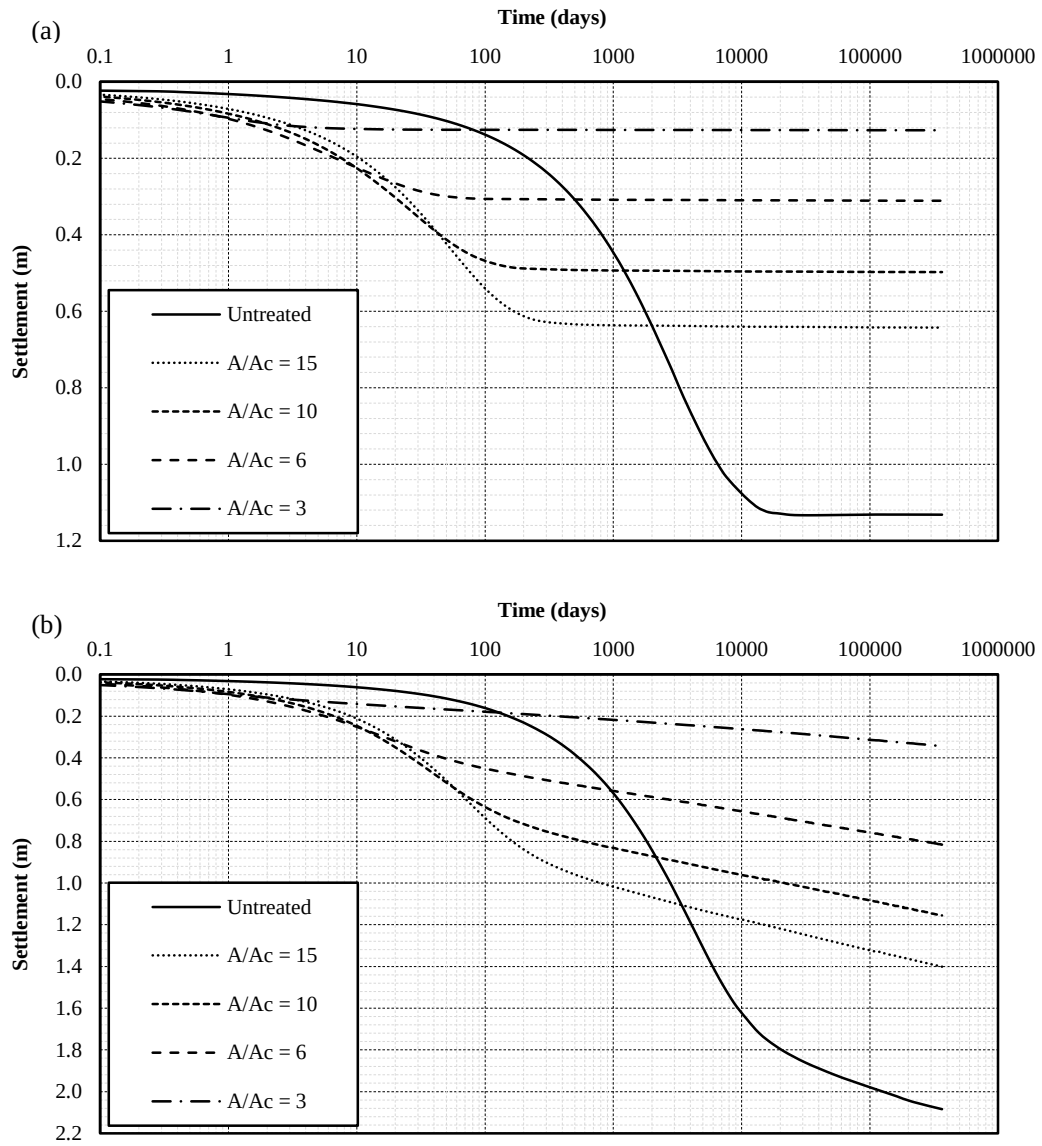

Fig. 5. Settlement vs. log(time) for the isotropic case (a) very low creep coefficient (b) standard creep coefficient

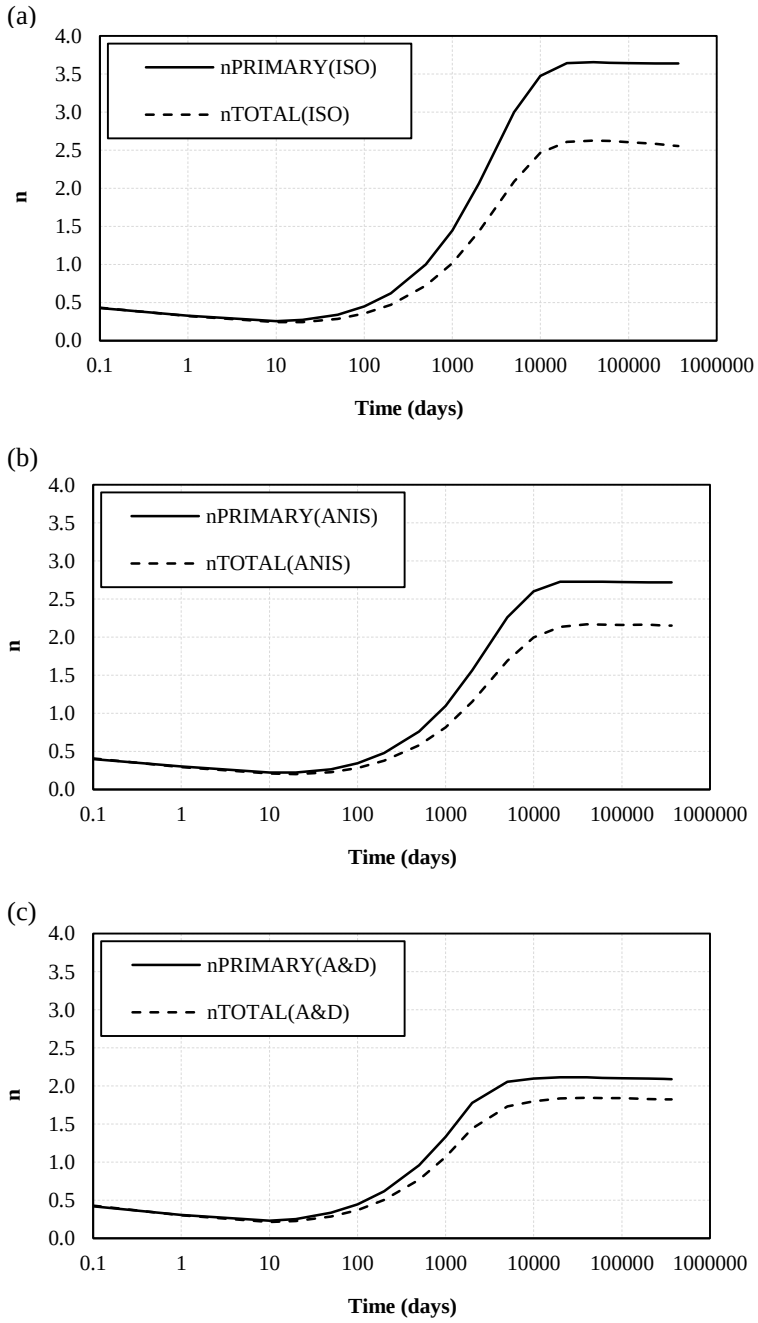

Fig. 6. Evolution of n with time at A/A_c = 6: (a) ISO (b) ANIS (c) A&D

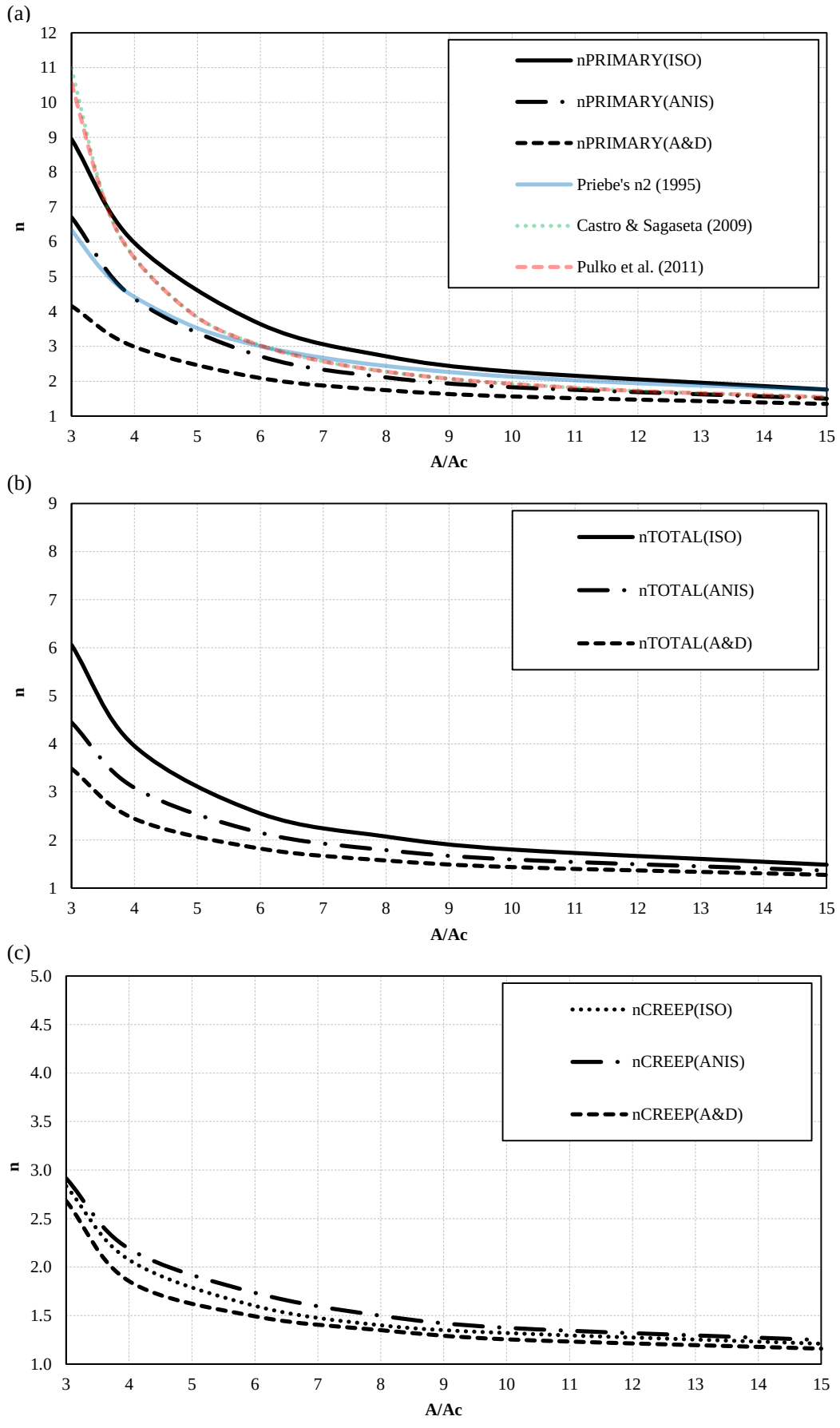

Fig. 7. (a) Comparison of $n_{PRIMARY}$ values (b) Comparison of n_{TOTAL} values (c) Comparison of n_{CREEP} values

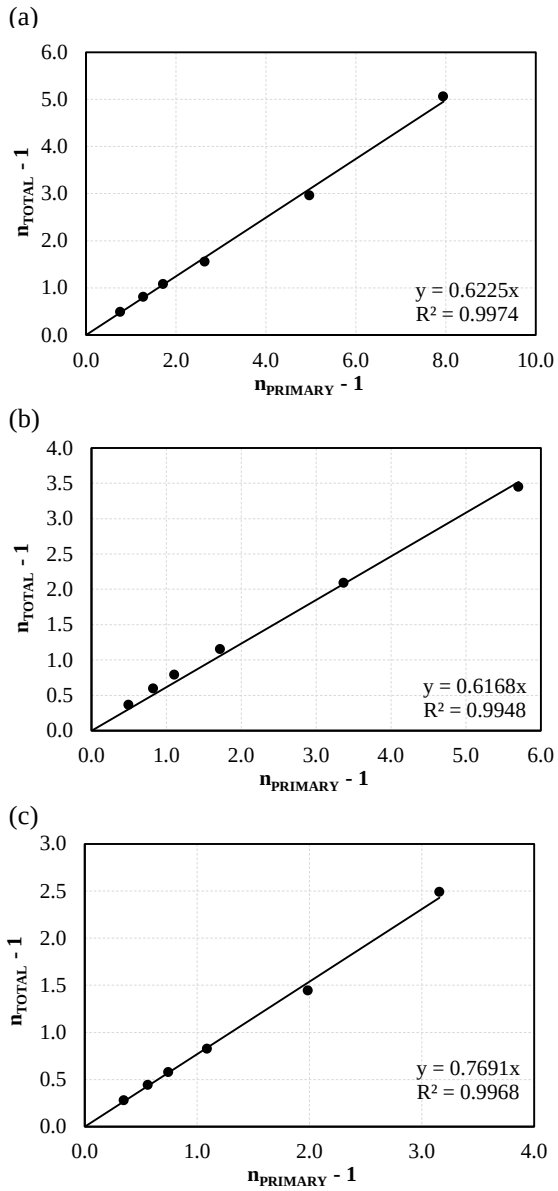

Fig. 8. (n_{TOTAL} - 1) vs. ($n_{PRIMARY}$ - 1) (a) ISO (b) ANIS (c) A&D

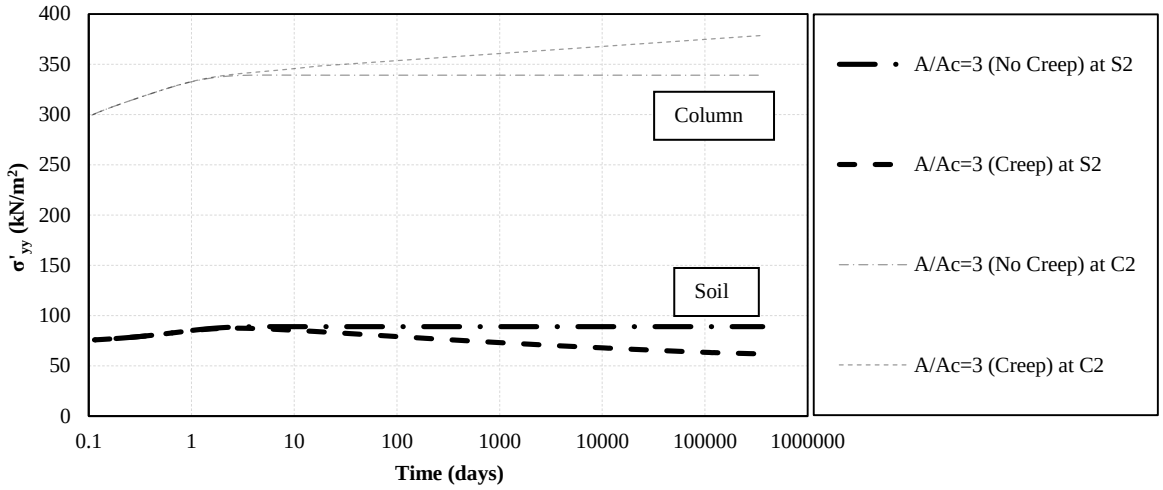

Fig. 9. Variation of vertical stress (σ'_{yy}) with time at mid-depth for the isotropic case

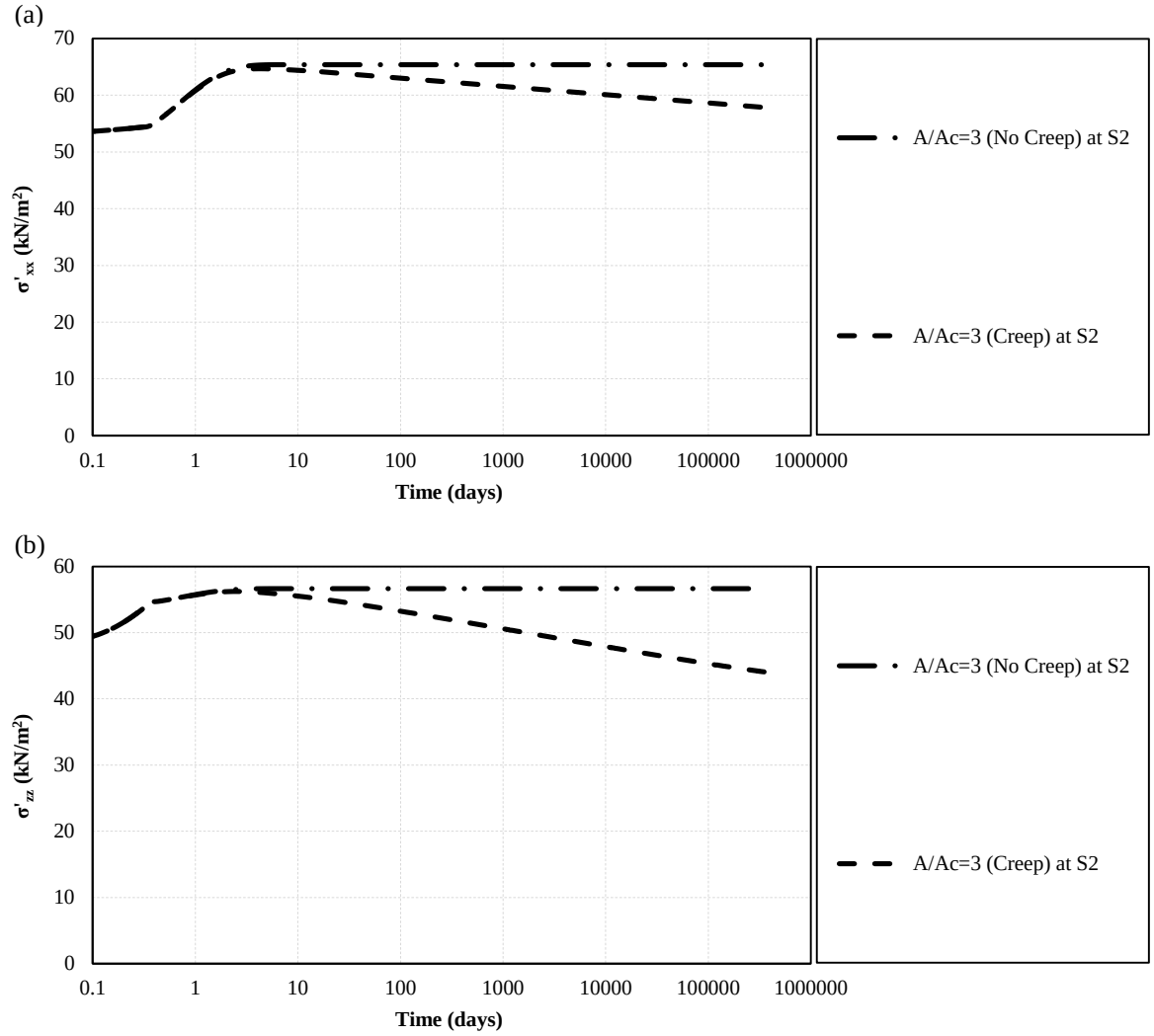

Fig. 10. Variations of (a) radial stress (σ'_{xx}) and (b) hoop stress (σ'_{zz}) in the soil with time at mid-depth

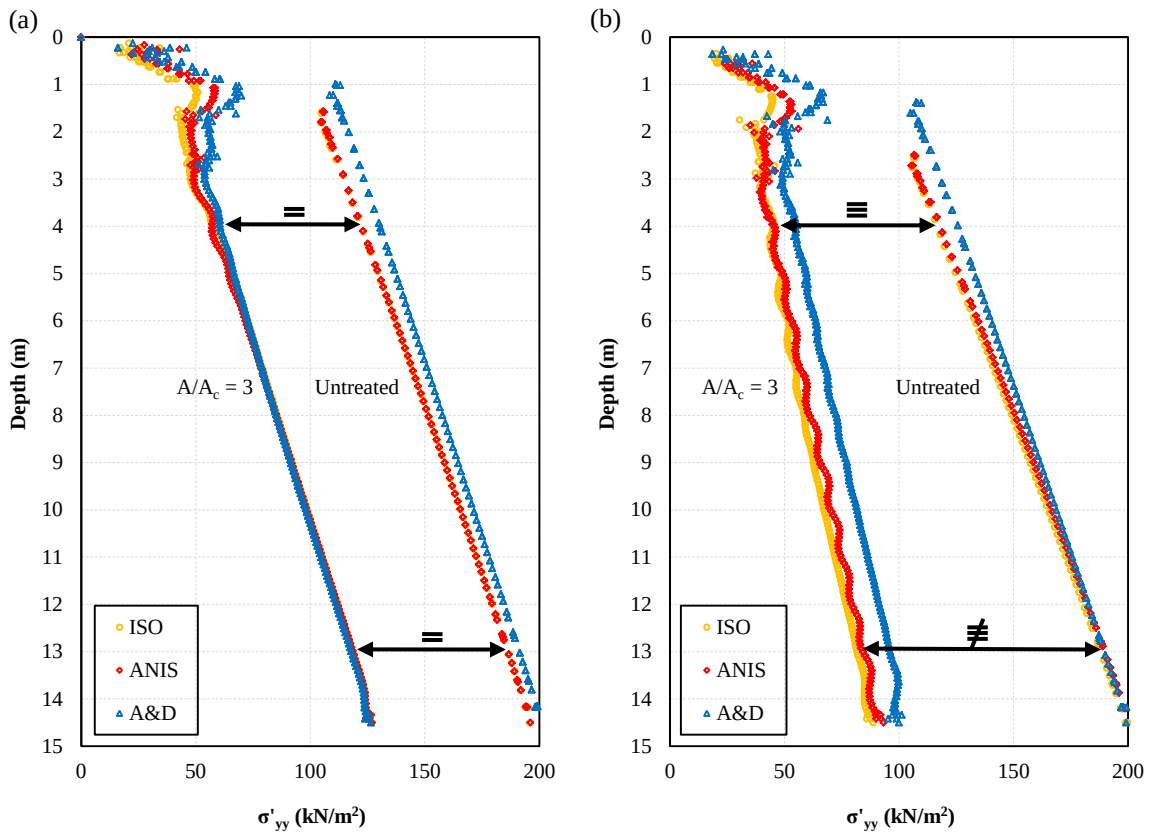

Fig. 11. Profiles of vertical stress in the soil for A/A_c = 3 (a) No Creep (b) Creep

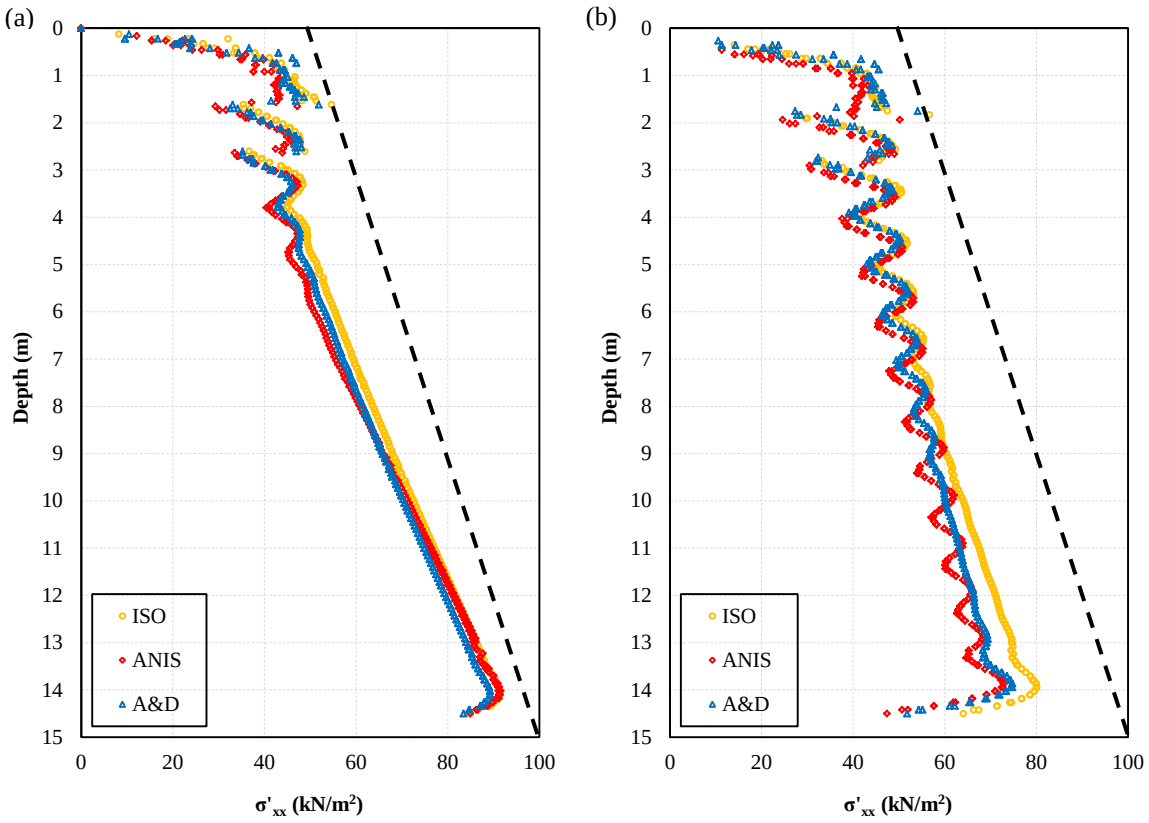

Fig. 12. Profiles of radial stress in the soil for A/A_c = 3 (a) No Creep (b) Creep

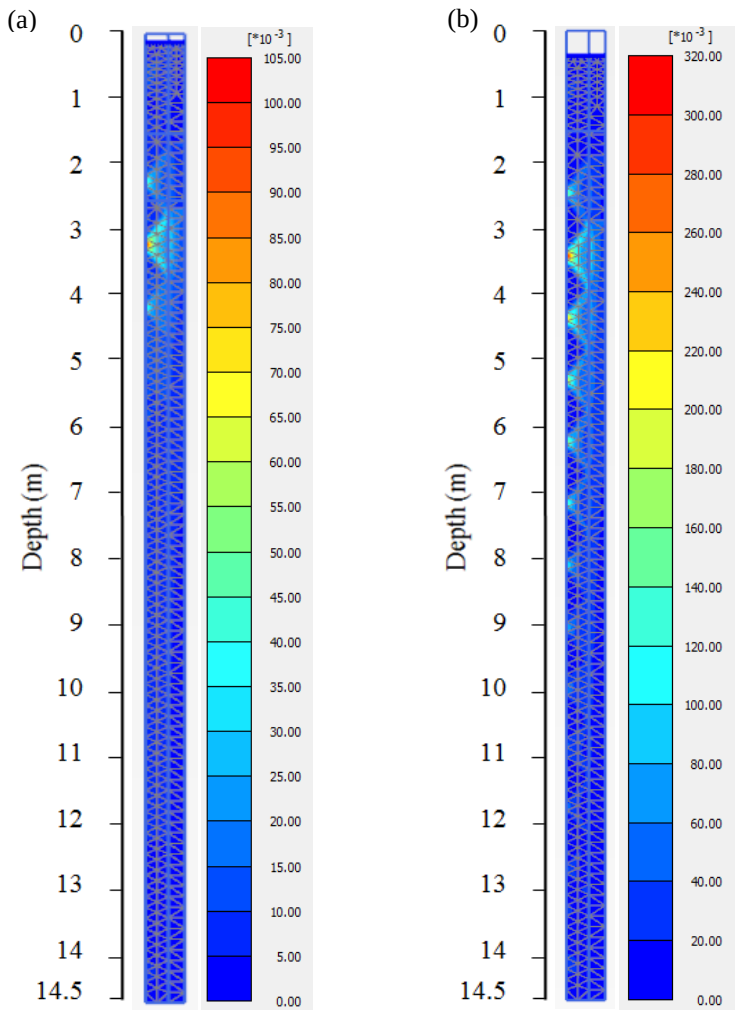

Fig. 13. Total shear strains for A/A_c = 3 (isotropic case) (a) No Creep (b) Creep

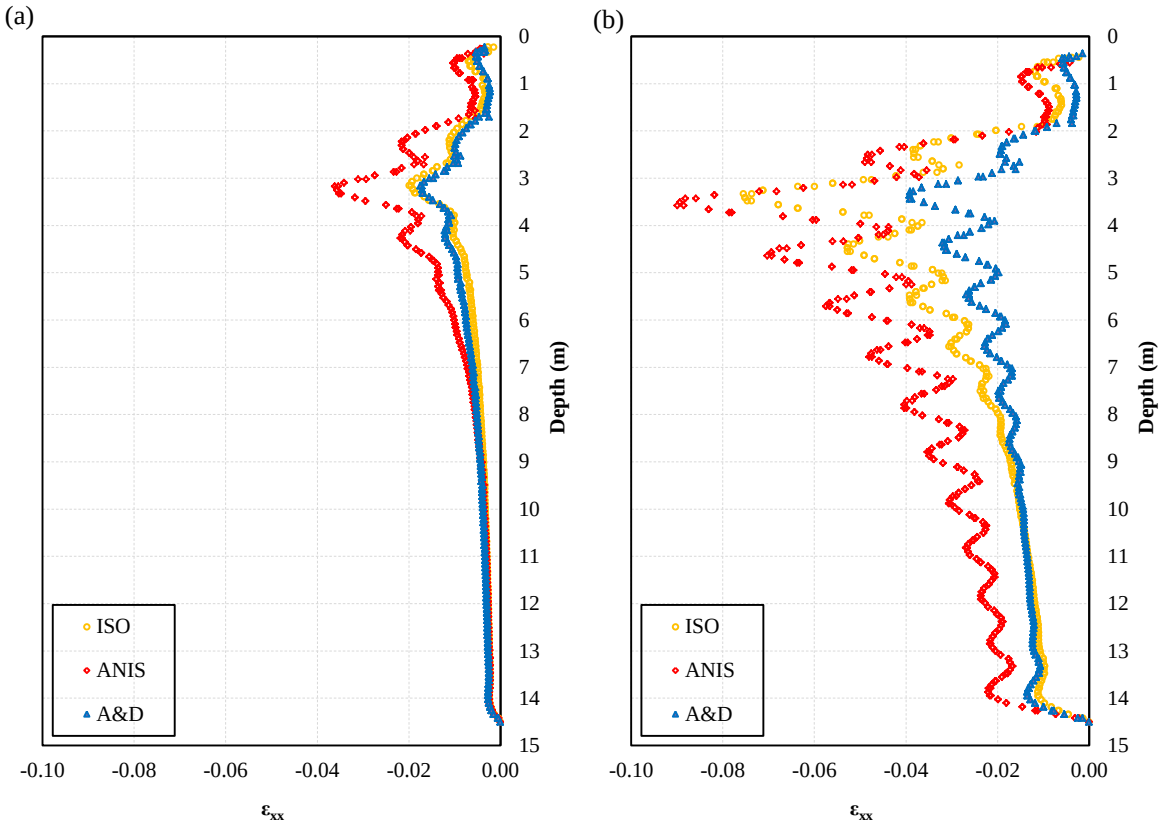

Fig. 14. Profiles of radial strain in the soil for A/A_c = 3 (a) No Creep (b) Creep

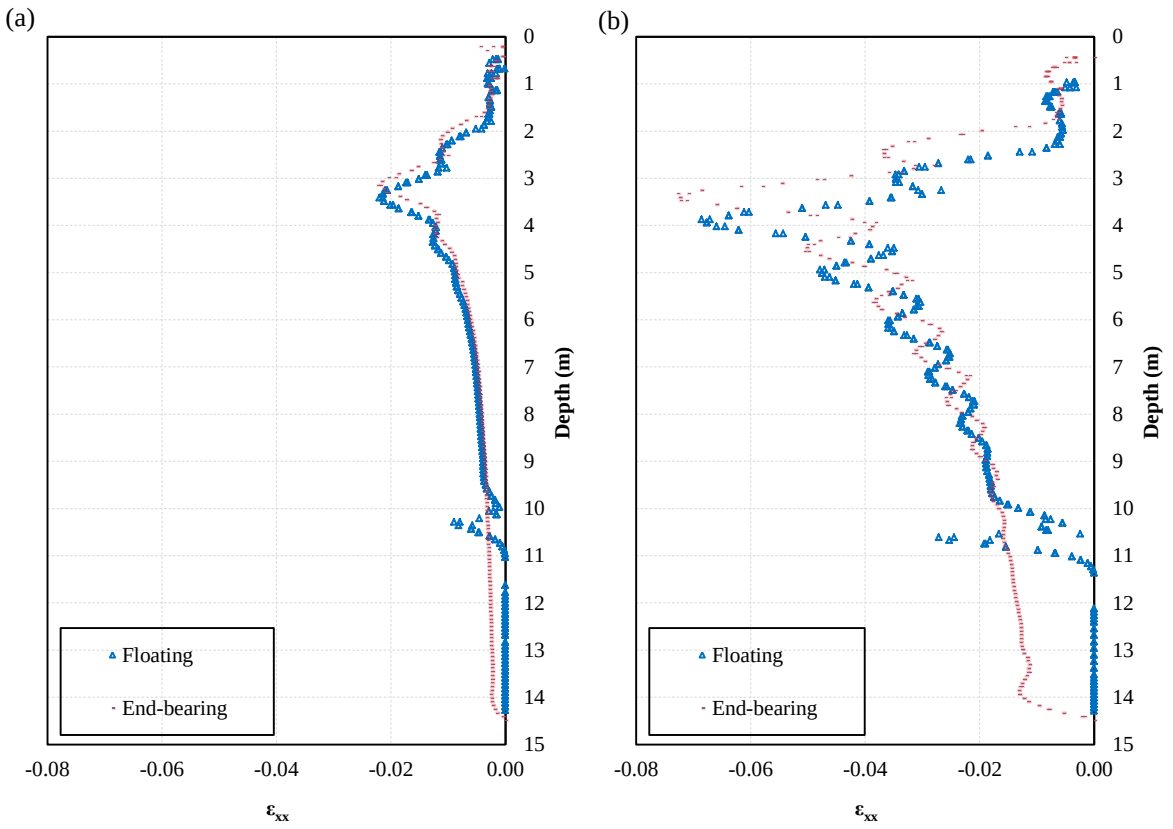

Fig. 15. Profiles of radial strain in the soil for A/A_c = 3 (isotropic case): floating vs. end-bearing columns (a) No Creep (b) Creep

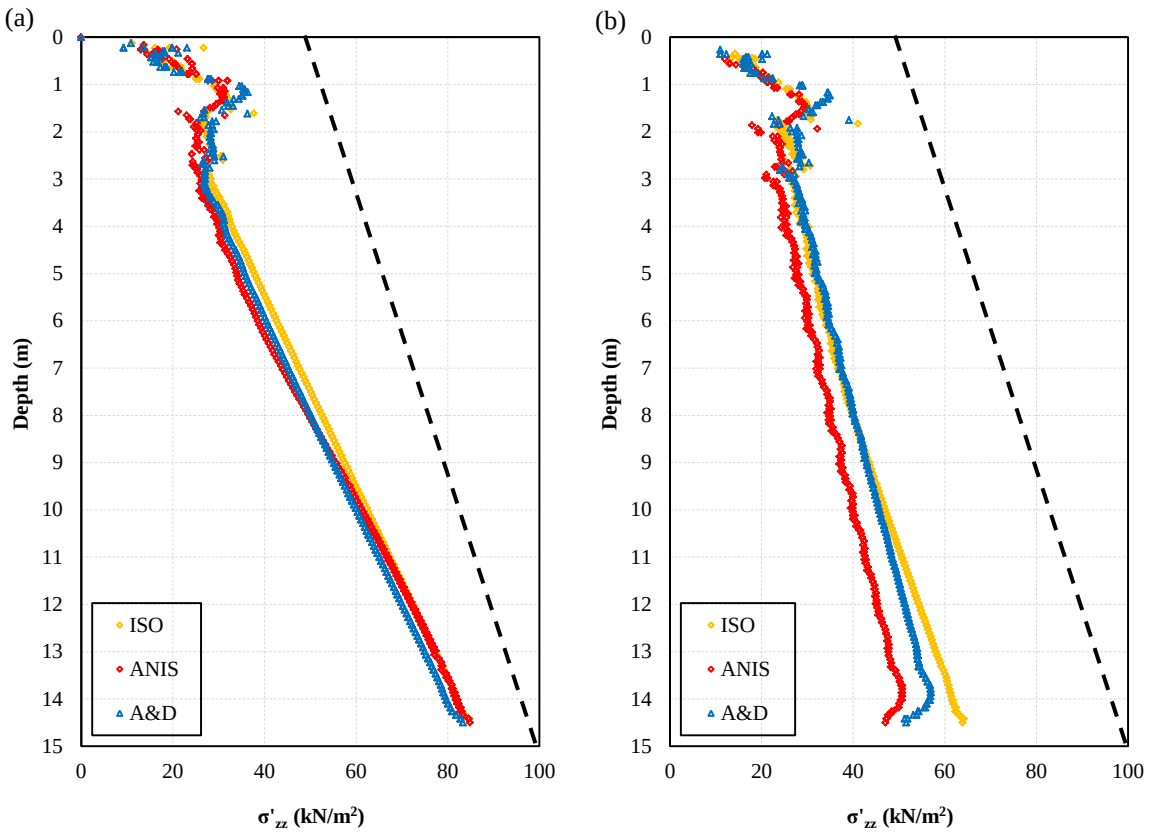

Fig. 16. Profiles of hoop stress in the soil for A/A_c = 3 (a) No Creep (b) Creep